Key Engineering Materials
ISSN: 1662-9795, Vol. 964, pp 157-162
doi:10.4028/p-HM0cq9

Submitted: 2023-06-06
Accepted: 2023-09-12
Online: 2023-11-23

Laser-Based Directed Energy Deposition of Ceramic Nanoadditivated AA7075 Powder Alloys

Rey, P.[1,a*], Lazaro, A.[1,b], Castro, G.[1,c], Sanchez, R.[1,d], Alleaume, C.[1,e], Prieto, C.[1,f], Pabel, T.[2,g] and Kaschnitz, E.[2,h]

[1]AIMEN Technology Centre, Polígono Industrial de Cataboi SUR-PPI-2 (Sector) 2, Parcela 3 E36418 - O Porriño, Spain.

[2]Österreichisches Gießerei-Institut, Parkstraße 21, 8700 Leoben, Austria.

[a]prey@aimen.es, [b]alejandro.lazaro@meltio3d.com, [c]gcastro@aimen.es, [d]raul.sanchez@aimen.es, [e]clovis.alleaume@aimen.es, [f]camilo.prieto@aimen.es, [g]thomas.pabel@ogi.at, [h]erhard.kaschnitz@ogi.at.

Keywords: Laser-based Directed Energy Deposition, 7075, aluminium alloys, ceramic nanoadditive.

Abstract. AA7075 is one of the most resistant aluminium alloys, so it is frequently used in very demanding industries as aeronautics or defence. However, the 7075 alloy falls into the non-weldable category thus hardly processable through additive manufacturing processes, and specially on laser-based DED (Directed Energy Deposition). The low absorption together with cracking behaviour remain a challenge for the industrialisation of these processes. Alloying with minor elements or addition of nano-reinforcement have been proven as a successful approach to increase its manufacturability. In this work, the feasibility of printing 7075 with nano-TiC as additive was evaluated. Two compositions with 0.5 and 2% in weight were developed by dry mixing. The powders were characterized by scanning electron microscopy (SEM) and flowability was compared with the unreinforced alloy. With the optimal laser process parameters, 3D coupons were printed to be characterized microstructurally, thermally, and mechanically. Process monitoring using thermal and high-speed cameras was carried out to gain insight into the thermal behaviour of the melt-pool and resulting process stability. After printing, aspect ratio of single tracks was measured, and dilution was also evaluated. Although addition of 0.5% of n-TiC promotes a slight improvement on the alloy, allowing it to be mechanically tested, it still presents some defects as porosity. By increasing the content up to 2%, both the quality and the mechanical performance were enhanced significantly.

Introduction

High strength aluminium alloys, as 7075, have a strong potential for lightweight applications due to their high specific resistance. However, some applications are hindered due to the poor weldability of that alloys despite the effort of several researchers to optimize and understand the process [1-3]. In laser-based welding/AM technologies some problems are magnified, and more challenges arise due to poor laser absorption and very dynamic heating and solidification rates [4-6]. Therefore, in the last years, modification of aluminium composition become of interest in order to overcome all these issues. Introduction of nanoadditives can improve both heat dissipation and quality of the printed materials [7-10]. Some of the most popular ceramic additives used are TiC, TiB2 and TiN [10, 11, 12]. Methods to mix nanoadditives with aluminium matrices comprises salt melting, electrostatic assembly technique, wet and dry mixing being the last the most used. [8, 9, 10].

Therefore, in this paper, the effect of different TiC additions on a 7075 alloy matrix has been studied. The flowability measurements after dry mixing were carried out followed by the monitoring of the printing process to check the effect of the n-TiC on both melt pool and solidification rate. Experimental analyses of the cross section of tracks were made to establish a correlation between the effect of n-TiC on the dimensions of the melt pool together with the monitoring trials. Microstructural analysis in coupons have revealed that nanoparticles are effective on grain size controlling together with a large improvement on reducing of main defects as porosity and cracking. Finally, mechanical properties have been obtained.

Experimental Procedure

AA7075 powder (ECKA granules Germany GmbH) with a PSD between >45 <106 μm and chemical composition (wt%): Zn: 5.3; Mg: 2.7; Cu: 1.6; Cr: 0.23; Fe: 0.07; Mn:<0.01; Si:0.04; Ti: <0.01; Al (bal) was used. The nano titanium carbide (n-TiC) used as reinforcement was supplied by IoLiTec Nanomaterials, with a particle size of 20-30nm (D50), a purity of 99% and a chemical composition of (wt%): C: 19.91; Fe: 0.20: N: 0.30; O: 0.85; Ti: bal. AA7075 was mixed in a blender (Turbula) with n-TiC in two different concentrations: 0.5 and 2% (wt). YSZ ceramic balls (BPR 1.1) were used to improve adhesion between Al particles and n-TiC, Powder flowability was measured using a Hall funnel under the standard ASTM B213 – 13 and morphology, with a Scanning electron microscope (SEM) HITACHI S-4800 II equipped with EDS microanalysis systems.

A robotized DED cell used consisted of a 6 axes ABB IRB4400 robot, a 16kW TruDisk laser (TRUMPF), a laser head, BEO D70 (TRUMPF) with a coaxial nozzle COAX 8 (FHG-IWS) and powder feeder GTV. Laser beam spot diameter was set at 2mm and the powder flow at 2g/min, using argon as carrier and protective gas (3 & 20L/min respectively). Optimized laser power was 1.5kW and process speed was 10mm/s. 3D coupons have been fabricated with 40 layers, 5 tracks per layer, using a raster path planning strategy. From these coupons, proportional tensile specimens were extracted (L_0=25mm and S_0= 19.56mm^2 being b_0= 6mm) and tested under UNE-EN ISO 6892-1:2017 in a universal machine SHIMADZU 250 kN. Optical micrographs (OM) were taken in a microscope OLYMPUS GX-71 and chemical attack to reveal grain size was Keller´s reagent. Also, thermal properties were analysed. The (apparent) heat capacity of the AA7075 without and with 2% n-TiC was measured by a heat-flow differential scanning calorimeter (DSC 404 F1 Pegasus, NETZSCH). Sapphire, as reference material for the heat flow rate calibration and platinum crucibles were used. The measurements were made at a constant heating/cooling rate of 10 K min^{-1} in argon (99.999 %). The thermal diffusivity of these two materials was also measured by two commercial laser-flash apparatus (NETZSCH, both type LFA 427) according to EN 821-2:1997 using pure argon. To improve the optical properties, the specimens were coated with thin graphite layer. A sapphire holder was used at higher temperatures above 550°C to support the softening specimens. The measured temperature increase at the backside of the specimen was fitted by a Cape-Lehmann-algorithm to correct for heat loss and laser pulse length.

To monitor the effect of the n-TiC on the melt pool, a coaxial thermal camera with a 64x64pixel 12bits MWIR Tachyon sensor (NIT) was used. Additionally, to record the tail cooling and nanoparticles influence, a high-speed camera placed off axis was implemented. A Photron Fastcam Mini AX200 with Navitar 12xZoomXtender optics was used for the data acquisition, allowing to capture video of up to 7000fps. An additional illumination combined with a notch filter on the camera is used to better visualize the process (Prizmatix UHP-F-LED LED emitting at 635 nm wavelength). A proprietary software has been developed by AIMEN to process the video and visualize through a colour map to distinguish oscillating melt pool areas of the statics ones. Warm colours represent moving images such as the waves of the melt pool. Monitoring trials have been carried out in five single tracks overlapped 100% for better consolidation of th melt pool. Confocal microscope and OM cross sections were used to address the effect of n-TiC on aspect ratio and dilution on the alloy.

Results and Discussion

Static flowability has been obtained for the three powders. The Hall flowability is a value that gives an idea about if a powder is going to flow or not under static conditions. Values obtained for the AA7075, AA7075+0.5%n-TiC and AA7075+2%n-TiC are 81.65, 72.46 and 67.18s/50g. Although nanoparticles normally flow worse, the reduction of the time to flow can be related with the smooth morphology achieved after mixing due to the use of balls to increase the mixing. Fig. 1 shows the SEM micrographs as an example for original 7075 powders and 7075 with 2% of n-TiC.

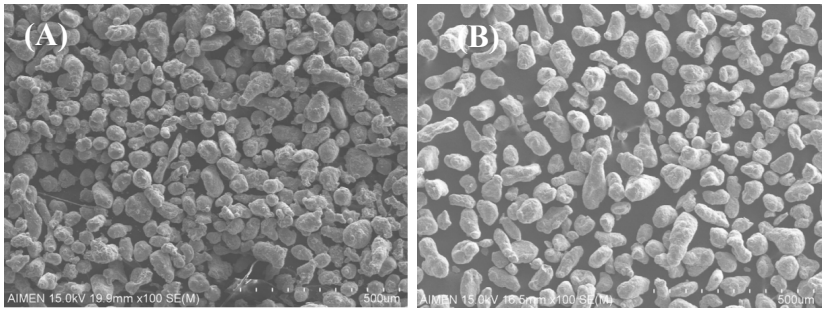

Fig. 1. SEM micrographs of AA7075 (A) and AA7075+2%n-TiC (B) particles.

Fig. 2 shows the effect of the nanoparticles on the dimensions of the single tracks for the two reinforced materials and the reference one. Fig. 3 shows the optical micrographs corresponding to the cross sections of 5 tracks overlapped 100%. In these micrographs it can better be observed how the dilution is increased (38% and 52%) as the tracks become wider (4% and 17%), while the height is reduced (26% and 38%) when the content of n-TiC is increased from AA7075 to 0.5% and 2% respectively. With 2% of n-TiC, porosity is reduced strongly.

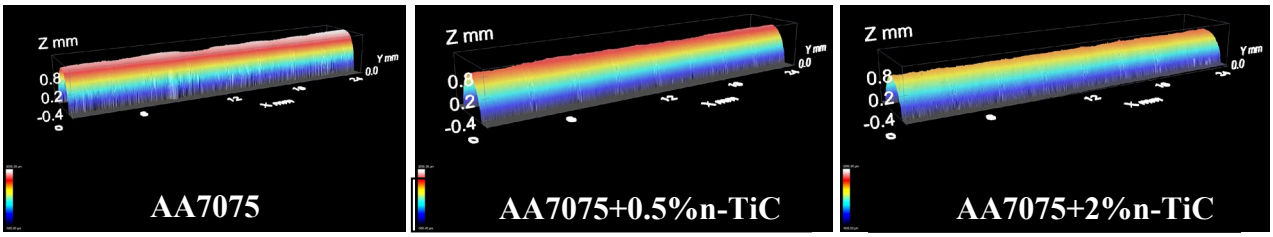

Fig.2. Confocal microscope graphs for the three materials tested.

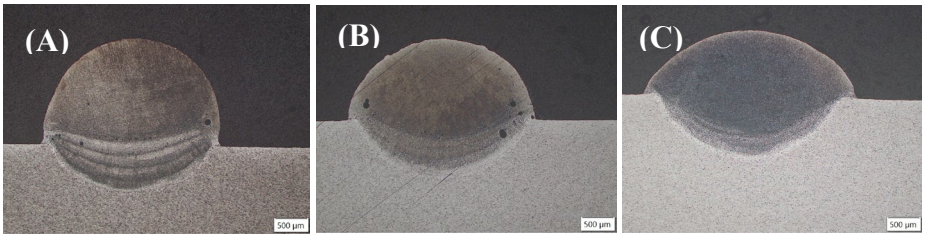

Fig. 3. Optical micrographs for cross sections of 5 tracks overlapped 100%, AA7075 (A), AA7075+0.5%n-TiC (B) and AA7075+2%n-TiC (C).

Figs. 4 & 5 represent the visual recordings used to monitor the melt pool and the melt pool+ tail acquired of the MWIR thermal camera and the high-speed camera, respectively, for the three materials in the last track of five´s overlapped 100%, to have a better consolidated melt pool.

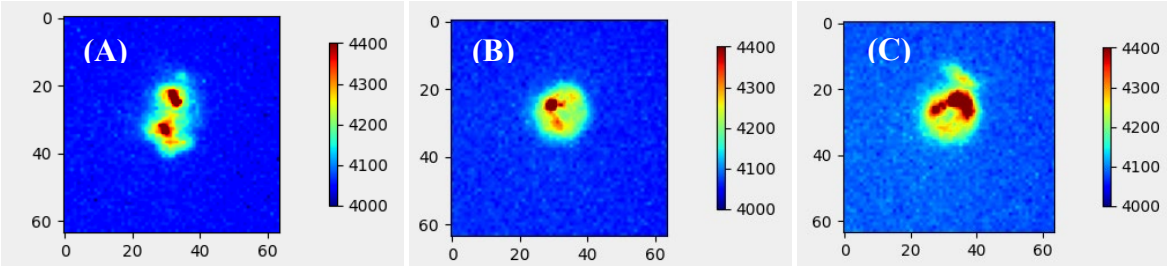

Fig. 4. False-colour image of thermal recordings with MWIR camera + AIMEN software [13] for AA7075 (A), AA7075+0.5%n-TiC (B) and AA7075+2%n-TiC (C).

Fig. 4 shows how the melt pool morphology changes with the TiC nanoparticles addition. Also, the melt pool becomes hotter as the n-TiC concentration is larger. In Fig. 5, the stillness of the video is studied through time, with warm colour representing a change of the pixel value during a given time window. With this representation, the corresponding tail is better observed as the melt-pool

presents waves, and therefore changes of the pixel intensity. As consequence of the ceramic addition, thermal conductivity is decreased promoting the enlargement of the tail (thermal conductivity of TiC is around 6 times lower [14,15] due to the reduction of cooling speed. Again, the widening of the tracks during the manufacturing is observed.

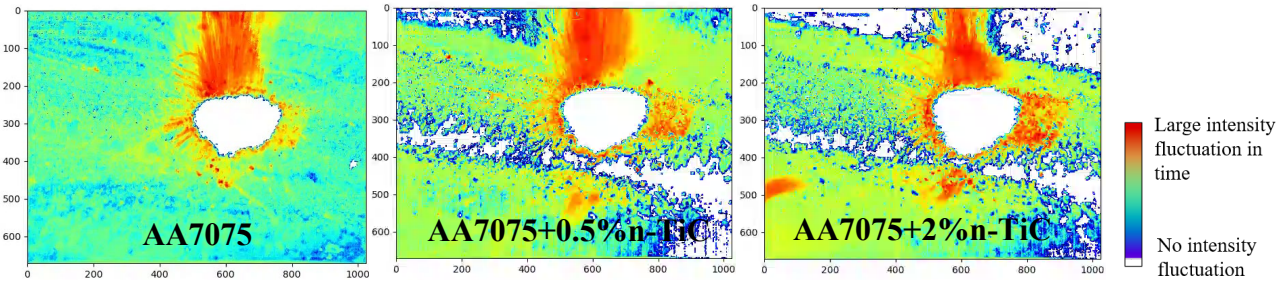

Fig. 5. False-colour images representing image stillness through time, for optic recordings with high-speed camera on the GUI developed by AIMEN for the three materials.

.

The effect of n-TiC on 7075 alloy is also shown in its thermal properties. Fig. 6 shows the apparent heat capacity for the alloy and the one reinforced with 2% of n-TiC. The most significant difference is the incipient melting; the pure aluminium alloy 7075 shows only one peak in the vicinity of the solidus temperature while the aluminium alloy 7075 with 2% n-TiC shows two smaller peaks. In the nano-reinforced one, the incipient melting happens faster, that might be attributed to a finer grain structure (see Fig. 9). On the other hand, thermal diffusivity is also affected by nanoparticles. The most important difference is in the solid phase, showing a higher thermal diffusivity (and conductivity) for pure AA7075 than for the nano-reinforced, while at melting, the difference vanishes. Therefore, AA7075 shows a higher capacity to cool down quickly.

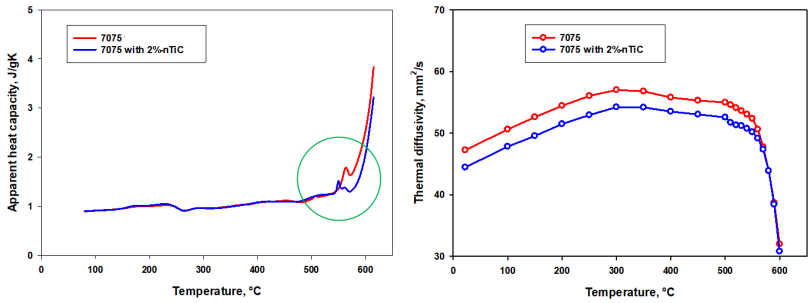

Fig. 6. Heat capacity and thermal diffusivity comparison of AA7075 and AA7075+2%n-TiC.

Fig. 7 shows the OM macrographs corresponding to printed coupons for the three materials. The best quality is presented by the third material although the deformation on the central part is higher due to the strong dilution. The 0.5% n-TiC promotes a big porosity but no large cracks are visible. Although 7075 coupon seems good, a lot of small cracks are in the whole coupon making it un-testable. OM micrographs without chemical attack taken on the central part of the coupons for the three materials are shown in Fig. 8, in which the defects are better visible. Fig. 9 shows chemically attacked optical micrographs to reveal the grain. The grain size has been reduced considerably, above all with 2% of n-TiC. With 0.5%, bi-modal structure can be observed with smaller and larger grains coexisting, showing an insufficient pinning effect to restrain the grain growth.

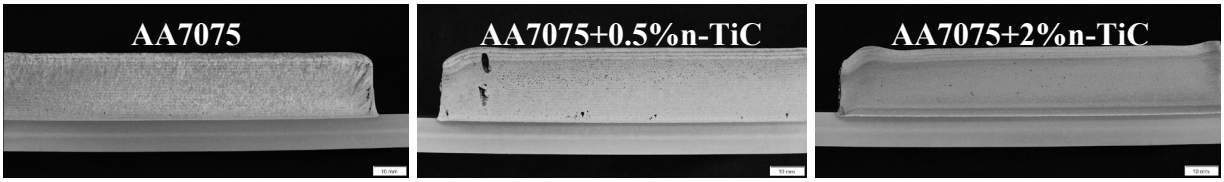

Fig. 7. OM macrographs of the coupons printed to extract tensile specimens.

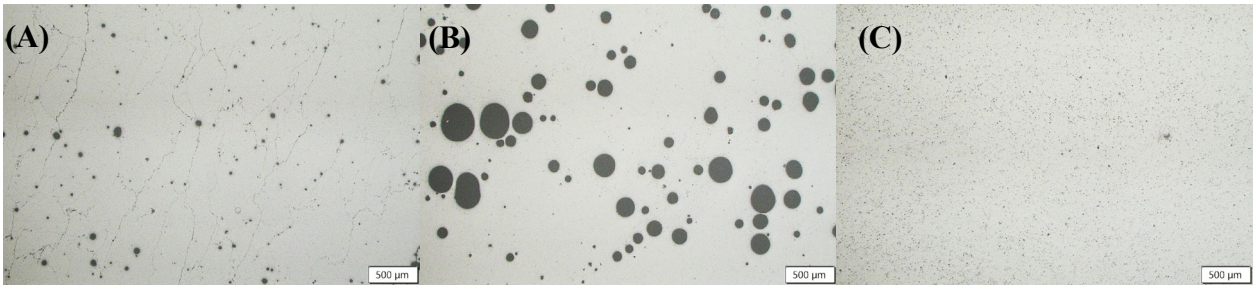

Fig. 8. OM micrographs of the central part of the coupons printed for the AA7075 (A), AA7075+0.5%n-TiC (B) and AA7075+2%n-TiC (C).

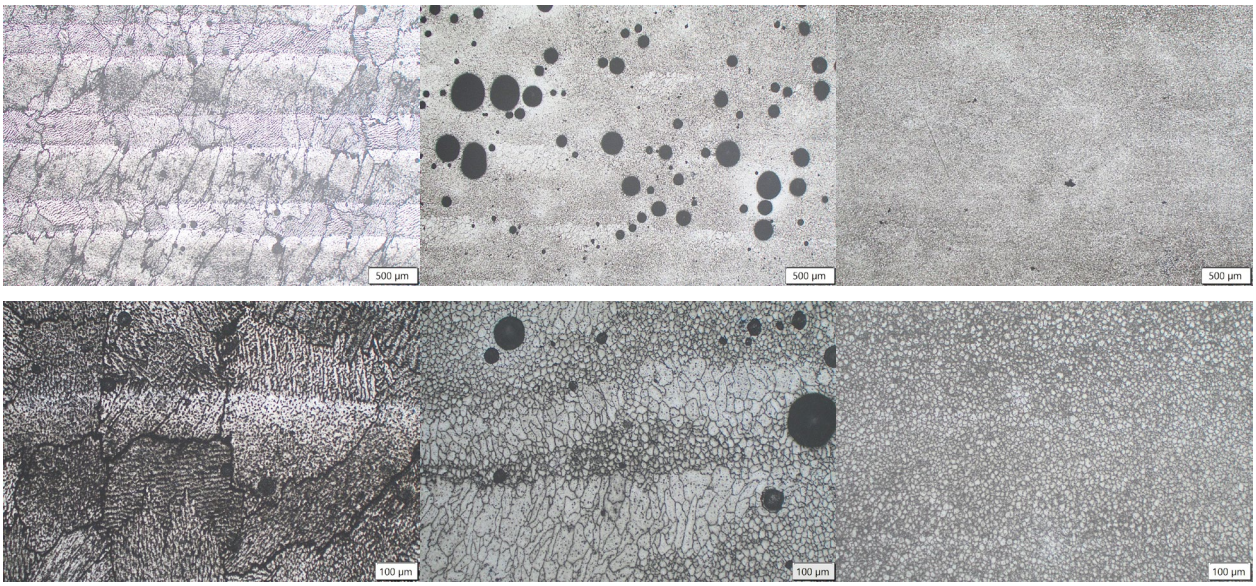

Fig. 9. OM micrographs different magnification (25 and 100x top and bottom respectively) for AA7075 (left), AA7075+0.5%n-TiC (middle) and AA7075+2%n-TiC (right).

The main effect of nano-additives on 7075 alloy is the thermal control under the printing process converting this non-weldable alloy in printable. TiC nanoparticles promotes a better compatibility of the 7075 alloy with the thermal cycles and fast cooling rate favouring and reducing both porosity and hot cracks. Additionally, n-TiC generate a more isotropic microstructure converting columnar grains into finer equiaxed ones. The improvement on the quality of the printed materials is translated into an enhancement of the tensile mechanical properties of the alloy (see Table 1). Although the YS is not very different for both nano-reinforced alloys, the better quality of the 2%n-TiC material is very well represented by the UTS and E. The low value of YS expected for the 2% could be related with the anisotropic dispersion of the n-TiC together with potential agglomeration. In any case, as being a hardenable alloy, full potential only can be achieved through a thermal treatment like T6.

Table 1. Mechanical properties for the three materials printed

Material	YS [Mpa]	UTS [MPa]	E [%]
AA7075	Not testable due to the multiple cracks		
AA7075+0.5%n-TiC	173.5±20.1	251.8±10.8	6.3±1.2
AA7075+2%n-TiC	177.3±19.8	330.8±18.9	13.4±1.4

Conclusions

Powdered reinforced AA7075 alloys were prepared using n-TiC particles with two different percentages by a dry mixing process. This process has no detrimental effects on the flowability of the powders making them suitable for DED printing.

These powders were used successfully to print tracks to be monitored showing that nanoparticles promote a strong effect on the melt pool widening, also reducing the cooling speed. Consequently, the width is increased, and the height reduced.

Nanoparticles act as nuclei agent modifying the constitutional undercooling rate promoting coupons without porosity and cracks. 0.5% n-TiC is not sufficient to suppress porosity completely but has a strong effect on crack removing. With a 2% n-TiC both defect types are completely removed showing an increase on tensile mechanical properties. These nano-additivities are able to convert a non-weldable alloy in a manufacturable one.

Acknowledgments

This work has been carried out under READI project (CER-20191020), funded by MICIIN/ CDTI and LIGHTME project (GA814552) funded by EU's Horizon 2020 research and innovation program.

References

[1] Pujari, K. S. & Patil, D. V. A review on GTAW technique for high strength aluminium alloys (AA 7xxx series), Int. J. Eng. Res. Technol. 2 8 (2013) 2477–2490.

[2] M. Holzer et al., Change of hot cracking susceptibility in welding of high strength aluminum alloy AA 7075, Physics Procedia 83 (2016) 463 – 471.

[3] Bekir Çevik, Gas tungsten arc welding of 7075 aluminum alloy: microstructure properties, impact strength, and weld defects, Mater. Res. Express, 5 (2018) 066540.

[4] Dixit, S.; Liu, S. Laser Additive Manufacturing of High-Strength Aluminum Alloys: Challenges and Strategies. J. Manuf. Mater. Process. 6 (2022) 156.

[5] Arnold Mauduit, et al., Study of the suitability of aluminum alloys for additive manufacturing by laser powder-bed fusion, U.P.B. Sci. Bull., Series B, 79 4 (2017) 219-238

[6] Sánchez Amaya JM. Laser welding of light metal alloys: aluminium and titanium alloys, Handbook of Laser Welding Technologies (2013) 215- 254.

[7] Sokoluk, M., Cao, C., Pan, S. et al. Nanoparticle-enabled phase control for arc welding of unweldable aluminum alloy 7075. Nat Commun 10 (2019) 98.

[8] Martin, J., et al. 3D printing of high-strength aluminium alloys, Nature 549 (2017) 365–369.

[9] Lin, TC., Cao, C., Sokoluk, M. et al. Aluminum with dispersed nanoparticles by laser additive manufacturing, Nat Commun. 10 (2019) 4124.

[10] Qu, M., Guo, Q., Escano, L.I. et al. Controlling process instability for defect lean metal additive manufacturing, Nat Commun 13 (2022) 1079.

[11] Xi, L.; et al., Microstructure development, tribological property and underlying mechanism of laser additive manufactured submicro-TiB2 reinforced Al-based composites. J. Alloys Compd. 819 (2020) 152980.

[12] Wen, X. et al., Laser solid forming additive manufacturing TiB2 reinforced 2024Al composite: Microstructure and mechanical properties. Mater. Sci. Eng. A 745 (2019) 319–325.

[13] Information on https://zenodo.org/record/5469946#.ZGOrU0_P1PY.

[14] https://asm.matweb.com/search/SpecificMaterial.asp?bassnum=ma7075t6

[15] Shen, L., et al., Synergistic strengthening of FeCrNiCo high entropy alloys via micro-TiC and nano-SiC particles. Mater. Today Commun. (2021) 26 101729.